

Journal of Biomedical Optics

SPIEDigitalLibrary.org/jbo

Impact of the optical depth of field on cytogenetic image quality

Yuchen Qiu
Xiaodong Chen
Yuhua Li
Bin Zheng
Shibo Li
Wei R. Chen
Hong Liu



SPIE

Impact of the optical depth of field on cytogenetic image quality

Yuchen Qiu,^a Xiaodong Chen,^{a,b} Yuhua Li,^a Bin Zheng,^c Shibo Li,^d Wei R. Chen,^e and Hong Liu^a

^aUniversity of Oklahoma, Center for Bioengineering and School of Electrical and Computer Engineering, 660 Parrington Oval, Norman, Oklahoma 73019

^bTianjin University, College of Precision Instrument and Opto-electronics Engineering, Weijin Road, Tianjin 300072, China

^cUniversity of Pittsburgh, Department of Radiology, 3362 Fifth Avenue, Pittsburgh, Pennsylvania 15213

^dUniversity of Oklahoma Health Sciences Center, Department of Pediatrics, 1100 N. Lindsay, Oklahoma City, Oklahoma 73104

^eUniversity of Central Oklahoma, Department of Engineering and Physics, 100 North University Drive, Edmond, Oklahoma 73034

Abstract. In digital pathology, clinical specimen slides are converted into digital images by microscopic image scanners. Since random vibration and mechanical drifting are unavoidable on even high-precision moving stages, the optical depth of field (DOF) of microscopic systems may affect image quality, in particular when using an objective lens with high magnification power. The DOF of a microscopic system was theoretically analyzed and experimentally validated using standard resolution targets under 60× dry and 100× oil objective lenses, respectively. Then cytogenetic samples were imaged at in-focused and off-focused states to analyze the impact of DOF on the acquired image qualities. For the investigated system equipped with the 60× dry and 100× oil objective lenses, the theoretical estimation of the DOF are 0.855 μm and 0.703 μm , and the measured DOF are 3.0 μm and 1.8 μm , respectively. The observation reveals that the chromosomal bands of metaphase cells are distinguishable when images are acquired up to approximately 1.5 μm or 1 μm out of focus using the 60× dry and 100× oil objective lenses, respectively. The results of this investigation provide important designing trade-off parameters to optimize the digital microscopic image scanning systems in the future. © 2012 Society of Photo-Optical Instrumentation Engineers (SPIE). [DOI: 10.1117/1.JBO.17.9.096017]

Keywords: digital pathology; depth of field, cytogenetic image quality.

Paper 12192P received Mar. 23, 2012; revised manuscript received Aug. 13, 2012; accepted for publication Aug. 23, 2012; published online Sep. 18, 2012.

1 Introduction

In digital pathology, high throughput digital microscopic image scanning is a fundamental technique for the diagnosis of various diseases.^{1–10} For this technique, however, one of the technical challenges is to maintain the pathologic specimen in focus during the image scanning, which may affect the reliability and efficiency of the image acquisition. The off-focused images can be attributed to several different factors, including the narrow depth of field (DOF) of an optical imaging system, and the impact of mechanical drifting and random vibrations of a scanning stage. These factors are often unavoidable even when using high-precision moving stages that may blur the scanned images. Although researchers continue to develop a precise focusing trace technique for high-quality microscopic image scanners, it is still necessary to understand the impact of the DOF on the scanned digital images. To do so will help balance the trade-off between scanning efficiency and image quality in the design of cost-effective digital microscopic image scanners.

This study aims to systematically investigate the tolerance level of off-focusing in diagnostic cytogenetic images. For this purpose, we first analyzed optical DOF of a microscope in theory. Then we measured the DOF using a standard resolution target under objective lenses with different magnification powers and numerical apertures (NA). After that, cytogenetic images from different clinical specimens were acquired and

analyzed using the same microscope equipped with a 60× (dry, NA = 0.95) and a 100× objective lenses (oil, NA = 1.25), respectively. The chromosomal band sharpness was subjectively assessed to investigate the image quality deterioration when the metaphase or interphase cells were captured at in-focused and off-focused states. The detailed experimental procedures and image quality analysis results are presented in this article.

2 Materials and Methods

2.1 Theoretical Analysis of DOF

The DOF of an optical system is defined as the axial range in the object space where the object is imaged with an acceptable deterioration.¹¹ There are two different types of DOF which contribute to the system DOF: geometric and diffractive. The geometric DOF is the axial range in the object space within which the blurred spot on the image space cannot be distinguished by the detector. It can be calculated by the following formula:¹¹

$$\Delta_g = \frac{2n}{\beta \text{NA}} p, \quad (1)$$

where n is the refractive index in the object space, β and NA are the magnification and numerical aperture of objective lens, and p is the pixel size of the detector.

The diffractive DOF is based on the light intensity distribution along the optical axis. The image deterioration is considered

Address all correspondence to: Hong Liu, University of Oklahoma, Center for Bioengineering and School of Electrical and Computer Engineering, 110 W. Boyd Street, Norman, Oklahoma 73019. E-mail: liu@ou.edu

to be acceptable if the intensity does not fall below 80% of the maximum. The corresponding distance can be computed as follows:¹¹

$$\Delta_d = \frac{n\lambda_0}{NA^2}, \quad (2)$$

where n is the refractive index in object space, NA is the numerical aperture of objective lens, and λ_0 is the wavelength of the illumination. In this investigation, it is assumed to be $0.550 \mu\text{m}$.

Thus, for a realistic microscopic imaging system, both geometrical and diffractive effects exist simultaneously. The calculation of the total DOF has been thoroughly discussed in the last several decades.^{11–16} Although a standard method of determining the total DOF has not been established to date, the following method is the most recommended in this field to compute total DOF, which is the sum of the diffractive and geometric DOF:^{11–14}

$$\Delta_{\text{total}} = \frac{2n}{\beta NA} p + \frac{n\lambda_0}{NA^2}. \quad (3)$$

2.2 Measurements of DOF

During the microscopic imaging process, the contrast of the captured image decreases when the object is moved away from the focal plane.^{17,18} Measuring the contrasts at specific spatial frequencies is often performed in an effort to assess the microscopic image system.^{19–21} Accordingly, in this study the DOF of the microscopic system was investigated experimentally by measuring the contrast at in-focused and off-focused positions. The DOF can be estimated experimentally by determining the range where the contrast is larger than 80% of its maximum.¹⁷

In order to acquire digital images, we modified a conventional microscope by installing a time delay integration (TDI) detector that enables obtaining a pixel size of $7 \mu\text{m}$ in one dimension. The microscope is also equipped with two different objective lenses providing the magnification power of $60\times$ (dry, NA = 0.95) and $100\times$ (oil, NA = 1.25), respectively.

During the experiment, the DOF range was estimated separately when applying each of the above two objective lenses. The experiment was divided into three steps. First, we measured the modulation transfer function (MTF) to determine the spatial frequency for DOF estimation. MTF was accomplished by measuring the image contrast at a series of discrete spatial frequencies from 0 to the system-resolving limit, with the measured contrast values normalized for the final MTF curve. Second, according to the MTF curve, the frequency where the contrast drops to half of the maximum was selected to estimate the DOF. Finally, at the selected frequency, the contrast was measured to determine the system DOF.

In order to determine the spatial frequency of a DOF estimation, the MTF was first measured using standard resolution targets. Two different bar pattern targets were used in the experiments. The USAF1951 resolution target contains different bar patterns with discrete spatial frequencies up to 645 lp/mm (USAF1951, Edmund Optics, NJ). Another target with maximal frequency of 2000 lp/mm was also applied to measure the contrast at spatial frequencies higher than 645 lp/mm when it is necessary (MRS-4, Geller Microanalytical Laboratory, MA.).

For each microscopic objective lens, the MTF was estimated through measuring the contrast at different spatial frequencies from 0 to the resolving limit. In this investigated system, the

pixel size of the camera is smaller than half of the resolving limit. Therefore, the spatial resolution is determined by the following formula:¹¹

$$\sigma = \frac{0.61\lambda_0}{NA}, \quad (4)$$

where NA is numerical aperture of the objective lens, and λ_0 is the wavelength of the illumination. In this investigation, it was assumed to be $0.55 \mu\text{m}$. Thus, when using the two objective lenses with $60\times$ and $100\times$ magnification power, the spatial resolution calculated with Eq. (4) is 0.353 and $0.268 \mu\text{m}$, or 1416 and 1863 lp/mm , respectively.

In the MTF measurement, the test target was placed on the stage. The system was manually adjusted to ensure that the target is imaged at the in-focused condition. After that, the target was captured and the contrast of each pattern on the target was calculated by the following formula:²²

$$C = \frac{I_{\text{max}} - I_{\text{min}}}{I_{\text{max}} + I_{\text{min}}}, \quad (5)$$

where I_{max} and I_{min} are the average maximum and minimum digital pixel values of the imaged test bar patterns at different frequencies. Based on the calculated contrasts at different spatial frequencies, the curve fitting method was then applied to create a smooth MTF curve.²³ The frequency where the MTF decreases to 0.5 is selected for the DOF estimation.

After the spatial frequency was determined, the DOF range was estimated for each objective lens. This was accomplished using the above test bar pattern targets. Before the measurement, the target was placed on the stage and the in-focused position was visually adjusted and determined. Then, starting from this in-focused position, the stage was gradually moved up and down with a series of steps. At each position, the target image was obtained by the detector and the contrast of the image is computed by Eq. (5). Finally, the calculated contrast was curved as a function of focusing positions. The range where the contrast is larger than 80% of the maximum is determined as the system DOF estimation.

2.3 Evaluation of the DOF Impact on the Cytogenetic Image Qualities

In this study, we selected multiple pathological specimen slides that cover a variety of clinical samples acquired from bone marrow, blood, amniotic fluid, and products of conception (POC). These collected samples were all prepared using the standard clinical procedure. The digital images were then acquired from these specimen slides' regions of interest (ROIs) to assess the impact of the microscope's DOF on the cytogenetic image qualities. Since the resolving power of the $60\times$ and $100\times$ objective lenses are $0.353 \mu\text{m}$ and $0.268 \mu\text{m}$, respectively, which provides enough meaningful information for clinical diagnosis, all the cytogenetic images were captured under these two $60\times$ and $100\times$ objective lenses in this study. Each ROI depicted an analyzable metaphase or interphase cell and each ROI was imaged at nine different positions, including the focal plane and the other positions away from the focal plane.

Table 1 The depth of field of our microscopic scanning system equipped with two different objective lenses.

Magnification	Type	Refractive index of object side	Numerical aperture (NA)	Detector pixel size	Geometric DOF	Diffractive DOF	System DOF
60x	Dry	1	0.95	7 μm	0.246 μm	0.609 μm	0.855 μm
100x	Oil	1.515	1.25	7 μm	0.170 μm	0.533 μm	0.703 μm

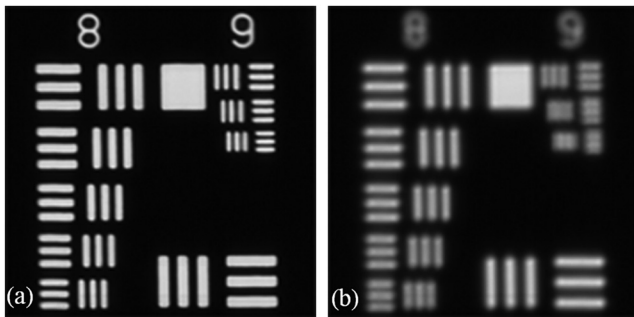


Fig. 1 Sample images of an USAF 1951 standard resolution target, acquired using a 100x (oil, NA = 1.25) objective lens including (a) in-focused image, (b) blurred image acquired 3.5 μm away from the focal plane.

3 Results

3.1 DOF Theoretical Results

The theoretical results calculated by Eq. (3) in Sec. 2.1 are tabulated in Table 1. The one-dimensional (1-D) pixel size of the CCD detector used in this system is 7 μm . When applying a dry 60x (NA = 0.95) microscopic objective lens and an oil-emerged 100x (NA = 1.25) objective lens, the computed system DOF are 0.855 and 0.703 μm , respectively. As expected, using higher magnification power results in a smaller DOF.

3.2 DOF Experimental Measurement

Two example images of the USAF1951 resolution test bar target are demonstrated in Fig. 1(a) and 1(b), which were captured at the focal position and 3.5 μm away from the focal plane of an

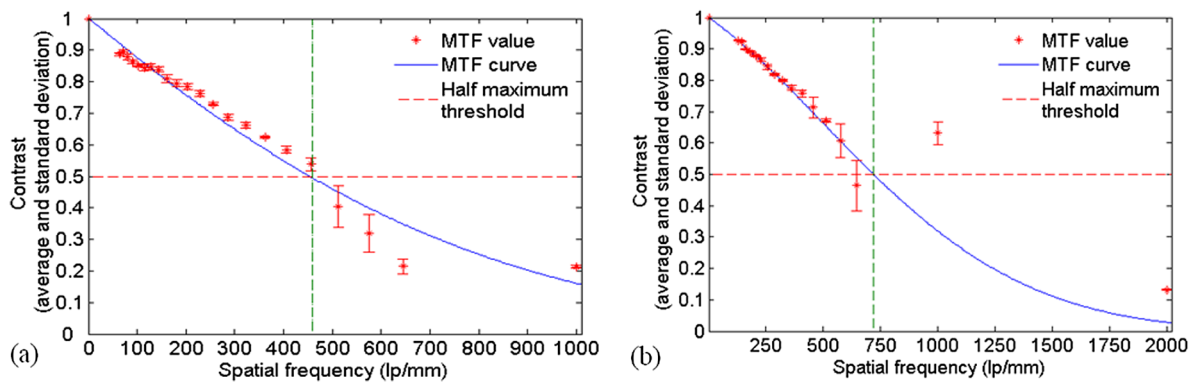


Fig. 2 The measured MTF curve for the tested microscope using (a) 60x (dry, NA = 0.95) objective lens and (b) 100x (oil, NA = 1.25) objective lens.

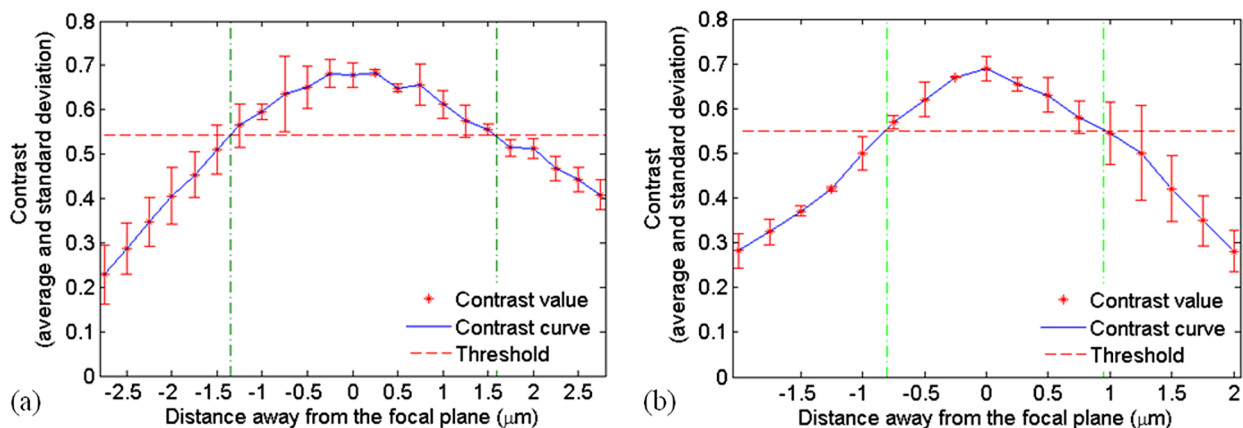


Fig. 3 The measured “half-maximum” contrast values versus focusing positions for the tested microscope using (a) 60x (dry, NA = 0.95) objective lens and (b) 100x (oil, NA = 1.25) objective lens.

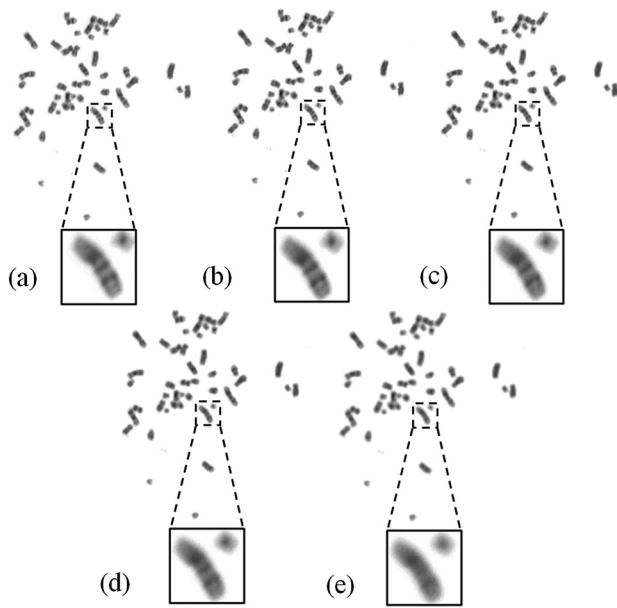


Fig. 4 Microscopic images of a clinically analyzable cell contained in a bone marrow sample, captured using a 60× objective lens (dry, NA = 0.95), at positions of (a) in-focused, (b) 1 μm , (c) 1.5 μm , (d) 2 μm , and (e) 2.5 μm away from the focal plane.

oil-emerged 100× objective lens, respectively. The image in Fig. 1(b) was acquired at the off-focused state, as it is obviously blurred. Figure 2 illustrates two measured MTF curves of the microscope when using two 60× and 100× objective lenses separately. Based on the measured MTF, the MTF decreases approximately to its half maximum value at 456 and 645 lp/mm, respectively. These spatial frequencies were therefore used to estimate the system DOF when the 60× and 100× objective lenses were applied.

The “half-maximum” contrast measurements, plotted as a function of focusing positions, are shown in Fig. 3(a) and 3(b),

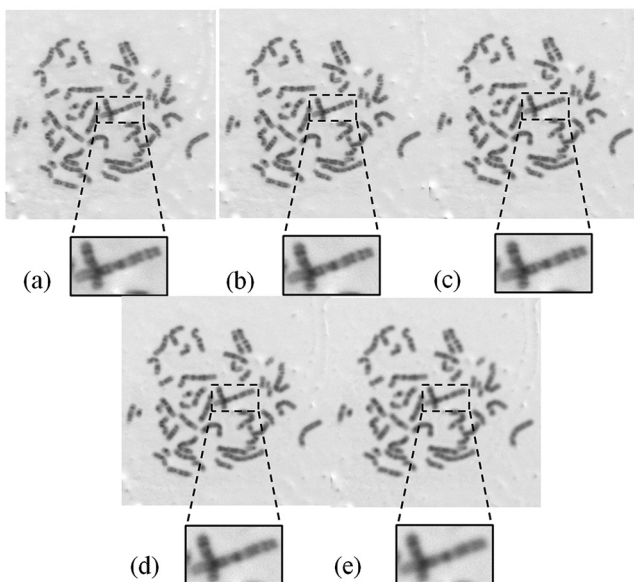


Fig. 5 Microscopic images of a clinically analyzable cell contained in a blood sample, captured using a 60× objective lens (dry, NA = 0.95), at positions of (a) in-focused, (b) 1 μm , (c) 1.5 μm , (d) 2 μm , and (e) 2.5 μm away from the focal plane.

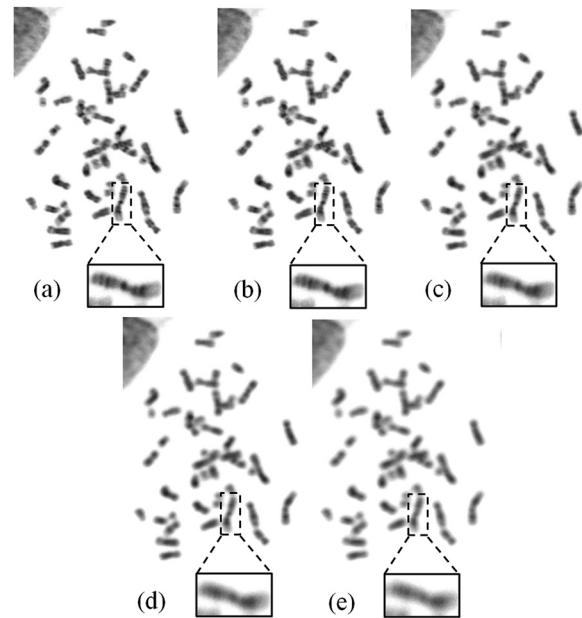


Fig. 6 Microscopic images of a clinically analyzable cell contained in a POC sample, captured using a 60× objective lens (dry, NA = 0.95), at positions of (a) in-focused, (b) 1 μm , (c) 1.5 μm , (d) 2 μm , and (e) 2.5 μm away from the focal plane.

when the 60× and 100× objective lenses were used, respectively. For each curve, the contrast value reaches its maximum at the in-focused position (0 at x -axis), and decreases as the target is moved away from the in-focused position. As mentioned, the DOF can be estimated as the range where the contrast is higher than 80% of its maximal value.¹⁷ Therefore, the actual

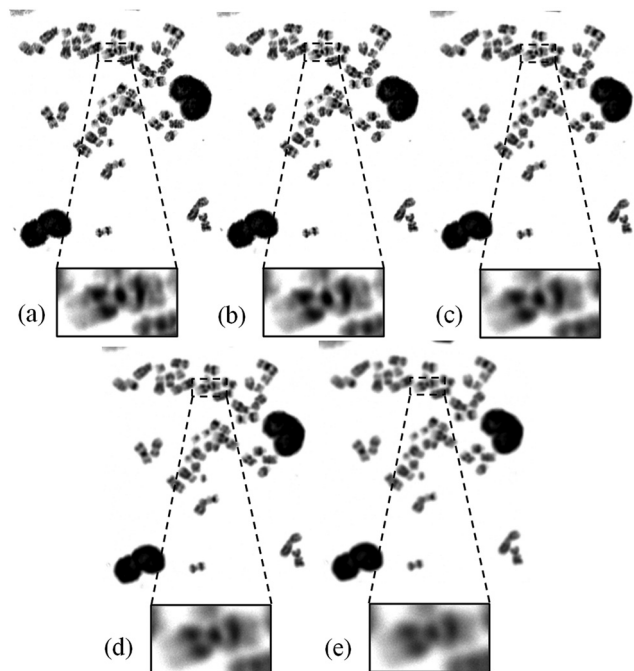


Fig. 7 Microscopic images of a clinically analyzable cell contained in a bone marrow sample, captured using a 100× objective lens (oil, NA = 1.25), at positions of (a) in-focused, (b) 0.5 μm , (c) 1 μm , (d) 1.5 μm , and (e) 2 μm away from the focal plane.

measured system DOF are $3.0\ \mu\text{m}$ and $1.8\ \mu\text{m}$ when applying the 60 \times and 100 \times objective lenses, respectively.

As predicted by theoretical calculations, the results reveal that the DOF decreases when increasing the NA. Due to the experimental restriction, the measured DOF is substantially greater than the theoretical prediction. In the experiment, we

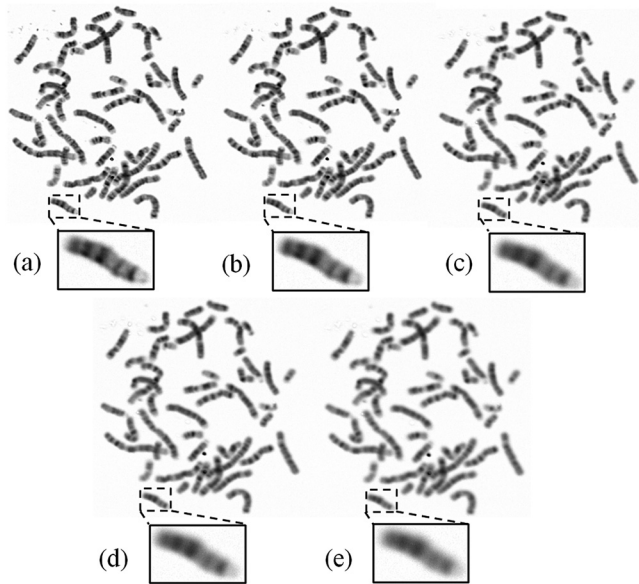


Fig. 8 Microscopic images of a clinically analyzable cell contained in a blood sample, captured using a 100 \times objective lens (oil, NA = 1.25), at positions of (a) in-focused, (b) $0.5\ \mu\text{m}$, (c) $1\ \mu\text{m}$, (d) $1.5\ \mu\text{m}$, and (e) $2\ \mu\text{m}$ away from the focal plane.

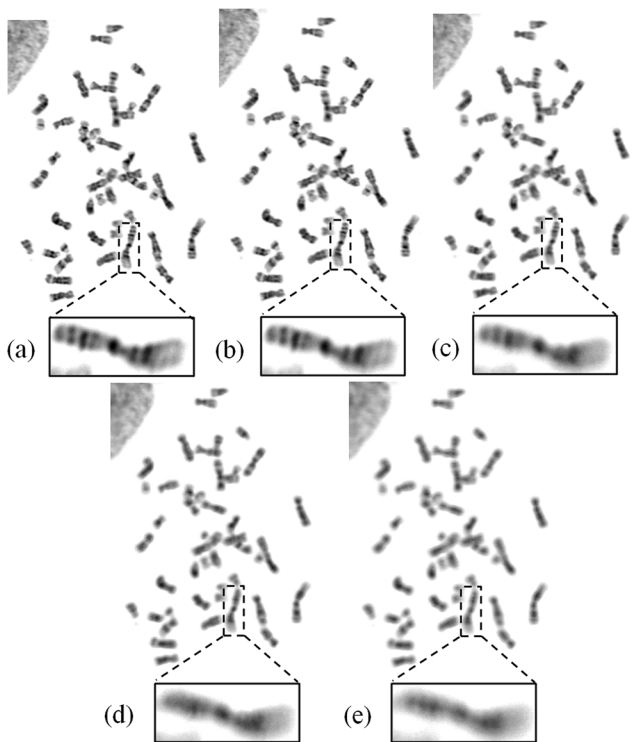


Fig. 9 Microscopic images of a clinically analyzable cell contained in a POC sample, captured using a 100 \times objective lens (oil, NA = 1.25), at positions of (a) in-focused, (b) $0.5\ \mu\text{m}$, (c) $1\ \mu\text{m}$, (d) $1.5\ \mu\text{m}$, and (e) $2\ \mu\text{m}$ away from the focal plane.

could not directly measure the size of the image spot or the axial light intensity for the geometrical and diffractive DOF separately. Alternatively, the DOF was estimated by measuring the image contrast. But the z -position where the image contrast drops to 80% of the maximum is not exactly the same position for the geometrical or diffractive DOF. In other words, theoretical computation can only be used as a reference.

3.3 DOF Impact on Diagnosis of Clinical Cytogenetic Images

The microscopic images of analyzable cells acquired from four pathological samples including bone marrow, blood, amniotic fluid, and POC are shown in Figs. 4 to 11 as examples. Figures 4 to 6 are metaphase cells acquired by the microscopic system using a 60 \times (dry, NA = 0.95) objective lens, and Figs. 7 to 10 are metaphase cells acquired under 100 \times (oil, NA = 1.25) objective lens. Figure 11 illustrates an interphase cell captured under a 100 \times (oil, NA = 1.25) objective lens. In each of Figs. 4 to 6, Image (a) was obtained at the focal plane resulting in clear and sharp chromosome band patterns, which are adequate for clinical diagnosis. Image (b) was acquired $1\ \mu\text{m}$ out of focus, and the band patterns are as clear as Image (a). When the cell was obtained $1.5\ \mu\text{m}$ away from the focal plane, the image is somewhat blurred but still recognizable, as shown in Image (c). The band contrast decreases more significantly when the cell moves further away from the focal plane, with the band shapes becoming barely recognizable and then totally unrecognizable in Image (d) and (e), both of which were acquired 2 and $2.5\ \mu\text{m}$ out of focus, respectively.

In Figs. 7 to 10, the band sharpness decreases at a faster rate as compared with those shown in Figs. 4 to 6. In Figs. 7 to 10, Image (c) was obtained $1\ \mu\text{m}$ away from the focal plane, which shows a cell containing somewhat recognizable band shapes with decreased contrast. However, these cells are still suitable for clinical practice. Furthermore, when the image was obtained

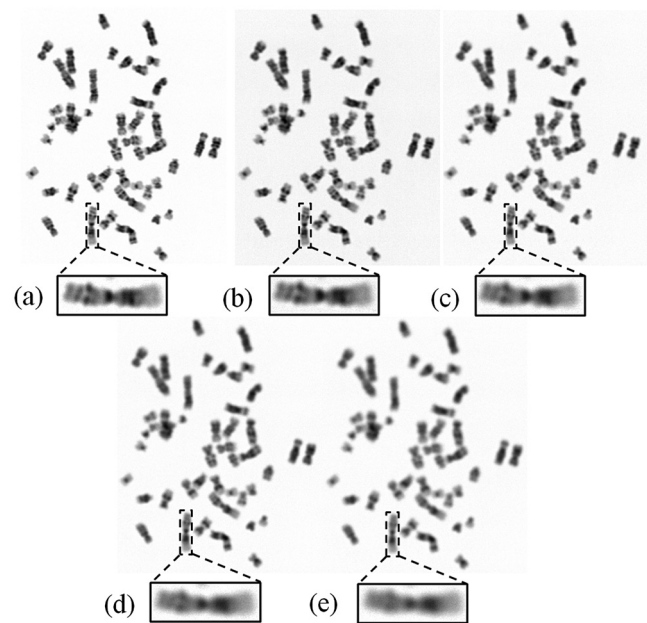


Fig. 10 Microscopic images of a clinically analyzable cell contained in an amniotic fluid sample, captured using a 100 \times objective lens (oil, NA = 1.25), at positions of (a) in-focused, (b) $0.5\ \mu\text{m}$, (c) $1\ \mu\text{m}$, (d) $1.5\ \mu\text{m}$, and (e) $2\ \mu\text{m}$ away from the focal plane.

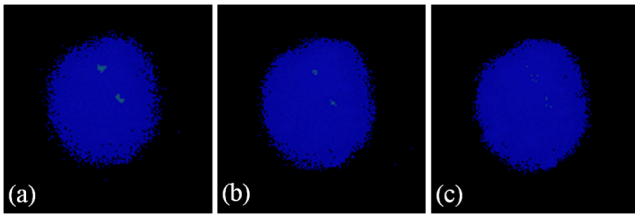


Fig. 11 Microscopic fluorescent *in situ* hybridization (FISH) images of a clinically analyzable interphase cell contained in a POC sample. The chromosomes of interest are marked as the fluorescent dots, and the cell is captured by the system under investigation using 100 \times objective lens (oil, NA = 1.25), at positions of (a) in-focused, (b) 1 μm , and (c) 2 μm away from the focal plane.

2 μm out of focus, the band patterns become completely unrecognizable and unsuitable for diagnosis purposes, as illustrated in Image (e).

Figure 11 shows a typical image of an interphase cell acquired from a POC sample. This cell was processed by the fluorescence *in situ* hybridization technique (FISH) biomarkers. The diagnostic genome fragments are demonstrated as bright dots in the captured image. The cell in Fig. 11(a) was imaged at the focal plane, and shows two clear green dots on the blue background. When the cell was moved 1 μm away from the focal plane, as shown in Fig. 11(b), the dots become smaller but still recognizable. However, the dots disappear completely in Fig. 11(c), which was captured 2 μm out of focus.

In summary, these experimental and observation results agree with the measured DOF ranges demonstrated in Sec. 3.2. For the investigated microscopic system, the range of DOF is approximately 3.0 μm and 1.8 μm when applying 60 \times (dry, NA = 0.95) and 100 \times (oil, NA = 1.25) objective lenses, respectively. The images acquired within DOF illustrate clearly cytogenetic features, which are adequate for the diagnosis of diseases in clinical practice. However, when the cell is moved out of the DOF range, the pathological meaning of the acquired images slowly diminishes.

4 Discussion and Conclusion

Pathological examination of clinical specimens provides ground truth of disease diagnosis. In clinical practice, there are many types of pathological tools to examine the abnormalities of tissue, cell, and chromosome.^{1-3,6-8} For example, consistent chromosome abnormalities have been proved to be associated with some serious diseases.¹⁻³ In order to diagnose these diseases, clinicians in the cytogenetic laboratories need to obtain in-focused images with clear and sharp chromosome bands, as the blurred bands in the digital images may result in misdiagnosis. For instance, among the karyotyping of metaphase chromosomes, the 21st trisomy is an important diagnostic evidence of Down's syndrome.² Since the size of 21st chromosome is shorter than the others, these chromosomes can be easily misunderstood as small debris in the off-focused state. In another example, Philadelphia translocation $t(9;22)(q34;q11)$, a reciprocal translocation between the 9th and 22nd chromosome, is highly related to chronic myelogenous leukemia.³ Clinicians need to locate the region q34 in the 9th chromosome and q11 in the 22nd chromosome by analyzing the band shape and counting the bands. In the off-focused image, however, the band shape becomes fuzzy; hence it is extremely difficult to distinguish between these two different regions, which might cause false positive or false negative results.

In order to ensure that the imaged chromosome bands are adequately sharp for the diagnosis, currently many microscopic systems perform the auto-focusing operation repeatedly for each useful cell.^{5,8} However, this method is often inefficient because the auto-focusing operation is quite time-consuming. Therefore, to balance the trade-off between the scanning efficiency and the image quality for a clinical diagnostic purpose, it is clinically meaningful to analyze how the DOF impacts on the acquired chromosome bands. To the best of our knowledge, no similar studies have been previously conducted and reported to investigate the tolerance level of out-focusing in automatically scanning pathological specimen slides.

In this study, we first computed DOF using a well-recognized theoretic model of an optical image system and then measured DOF of the same optical system using a standard test bar pattern target. Our results showed that the experimentally measured DOF was substantially greater than that computed by the theoretic model. This suggests the importance of using well-designed experiments to assess and measure the actual DOF of an optical system (e.g., a microscope). In addition to using the standard test bar target, we also analyzed DOF (or off-focusing tolerance level) by obtaining cytogenetic images under this specific microscope with two objective lenses of 60 \times (dry, NA = 0.95) and 100 \times (oil, NA = 1.25). Four types of commonly cytogenetic specimens acquired from bone marrow, blood, amniotic fluid, and POC in our cytogenetic laboratory were tested and analyzed in this study. Although the quality (i.e., sharpness and/or contrast of the metaphase chromosomes) of the images acquired from these four types of specimens varies, our experimental results demonstrated that the chromosomal band remained analyzable if the cells were captured within the range of 1.5 or 1.0 μm away from the focal plane when using the two 60 \times or 100 \times objective lenses, respectively. Comparing the experimental results acquired from using these two objective lenses, one could find that the microscopic system's DOF would be wider if low magnification objective lenses were utilized. However, the resolution of the pathological features also decreased. In summary, the results from this study support the feasibility of developing the automated microscopic or pathological image scanners with limited power of auto-focusing, which will significantly increase the efficiency of image scanning, as well as the efficacy of digital pathology.

Although the results of this preliminary study are encouraging, there are several limitations. First, we did not consider the effect of the chromosome thickness in this study.²⁴ Second, a simple DOF measurement was used and we did not test whether applying the new contrast calculation methods proposed recently could achieve more accurate results.²⁵⁻²⁹ Third, although the DOF of the human eye is also an important factor affecting subjective evaluation of the cytogenetic image qualities,^{30,31} it was not tested or discussed. Hence, a more comprehensive investigation is underway from which we hope to acquire better knowledge about the designing trade-off parameters to optimize the automated digital microscopic image scanning systems for cytogenetic image diagnosis and other digital pathology applications in the future.

Acknowledgments

This research is supported in part by the Grants CA115320 and CA136700 from the National Cancer Institute, National Institutes of Health, U.S.A. The authors would like to acknowledge the support of the Charles and Jean Smith Chair

endowment fund, as well. Both Yuchen Qiu and Xiaodong Chen are considered first authors.

References

1. J. H. Tjio and A. Levan, "The chromosome number of man," *Hereditas (Lund. Swed.)* **42**(1–2), 1–6 (1956).
2. J. Lejeune, M. Gautier, and R. Turpin, "Etudes des chromosomes somatiques de neuf enfants mongoliens," *CR Acad. Sci.* **248**(11), 1721–1722 (1959).
3. P. C. Nowell and D. A. Hungerford, "Minute chromosome in human chronic granulocytic leukemia," *Science* **132**(3438), 1497–1497 (1960).
4. M. J. Becich, "Why the future of medicine's gold standard is to go digital," presented in *SPIE Medical Imaging 2012*, San Diego, CA, <http://spie.org/x86306.xml> (4–9 February 2012).
5. J. Piper, E. Granum, D. Rutovitz, and H. Ruttledge, "Automation of chromosome analysis," *Signal Process.* **2**(3), 203–221 (1980).
6. G. M. Hampton et al., "Simultaneous assessment of loss of heterozygosity at multiple microsatellite loci using semi-automated fluorescence-based detection: subregional mapping of chromosome 4 in cervical carcinoma," *Proc. Natl. Acad. Sci. U. S. A.* **93**(13), 6704–6709 (1996).
7. K. Truong et al., "Quantitative fish determination of chromosome 3 arm imbalances in lung tumors by automated image cytometry," *Med. Sci. Monit.* **10**(11), 426–432 (2004).
8. B. Kajtar et al., "Automated fluorescent in situ hybridization (FISH) analysis of t(9;22)(q34;q11) in interphase nuclei," *Cytometry A* **69**(6), 506–514 (2006).
9. Y. C. Qiu et al., "Automated detection of analyzable metaphase chromosome cells depicted on scanned digital microscopic images," *Proc. SPIE* **7627**, 762718 (2010).
10. Y. C. Qiu et al., "An automatic scanning method for high throughput microscopic system to facilitate medical genetic diagnosis: an initial study," *Proc. SPIE* **8224**, 82240E (2012).
11. R. Oldenbourg and M. Shribak, "Microscopes," in *The Handbook of Optics*, 3rd ed., M. Bass and V. N. Mahajan, Eds., Vol. 1, pp. 28.18–23, McGraw-Hill Companies, New York (2010).
12. S. Inoue and K. R. Spring, *Video Microscopy: The Fundamentals*, 2nd ed., Plenum, New York and London (1997).
13. P. Horst, *Microscope Photometry*, Springer, New York and Berlin (1977).
14. L. C. Martin, *The Theory of Microscope*, Elsevier, New York (1966).
15. M. Born and E. Wolf, *Principles of Optics*, 5th ed., Pergamon, Oxford (1975).
16. H. Gross et al., *Handbook of Optical Systems*, Vol. 3, Wiley-VCH, Weinheim (2005).
17. H. H. Hopkins, "The frequency response of a defocused optical system," *Proc. R. Soc. London. Ser. A* **231**(1184), 91–103 (1955).
18. P. A. Stokseth, "Properties of a defocused optical system," *J. Opt. Soc. Am.* **59**(10), 1314–1321(1969).
19. M. C. Wood et al., "Using contrast transfer function to evaluate the effect of motion blur on microscope image quality," *Proc. SPIE* **6857**, 68570F (2008).
20. C. J. R. Sheppard, "Defocused transfer function for a partially coherent microscope and application to phase retrieval," *J. Opt. Soc. Am. A* **21**(5), 828–831 (2004).
21. A. N. Simonov and M. C. Rombach, "Asymptotic behavior of the spatial frequency response of an optical system with defocus and spherical aberration," *J. Opt. Soc. Am. A* **27**(12), 2563–2573 (2010).
22. W. J. Smith, *Modern Optical Engineering*, 4th ed., McGraw-Hill, New York (2008).
23. B. Bradie, *A Friendly Introduction to Numerical Analysis*, Pearson Education, New Jersey (2006).
24. A. Yamamoto et al., "Imaging of chromosomes at nanometer-scale resolution using soft X-Ray microscope at Ritsumeikan University SR Center," *J. Phys. Conf. Ser.* **186**(1), 1–3 (2009).
25. G. D. Boreman and S. Yang, "Modulation transfer function measurement using 3-bar and 4-bar targets," *Appl. Opt.* **34**(34), 8050–8052 (1995).
26. D. N. Sitter, J. S. Goddard, and R. K. Ferrell, "Method for the measurement of the modulation transfer function of sampled imaging systems from bar-target patterns," *Appl. Opt.* **34**(4), 746–751 (1995).
27. E. Marom, B. Milgrom, and N. Konforti, "Two-dimensional modulation transfer function: a new perspective," *Appl. Opt.* **49**(35), 6749–6755 (2010).
28. P. D. Lin and C. S. Liu, "Geometrical MTF computation method based on the irradiance model," *App. Phys. B Laser. Opt.* **102**(1), 243–249 (2011).
29. P. D. Lin and W. Wu, "Calculation of the modulation transfer function for object brightness distribution function oriented along any direction in axis-symmetrical optical systems," *Appl. Opt.* **50**(17), 2759–2772 (2011).
30. S. Marcos, E. Moreno, and R. Navarro, "The depth-of-field of the human eye from objective and subjective measurements," *Vision Research* **39**(12), 2039–2049 (1999).
31. Y. K. Nio et al., "Spherical and irregular aberrations are important for the optimal performance of the human eye," *Ophthal. Physiol. Opt.* **22**(2), 103–112 (2002).